# Ultrafast XANES Monitors Femtosecond Sequential Structural Evolution in Photoexcited Coenzyme $B_{12}$

Nicholas A. Miller,<sup>1</sup> Lindsay B. Michocki,<sup>1</sup> Arkaprabha Konar,<sup>2</sup> Roberto Alonso-Mori,<sup>3</sup> Aniruddha Deb,<sup>1,4</sup> James M. Glownia,<sup>3</sup> Danielle L. Sofferman,<sup>5</sup> Sanghoon Song,<sup>3</sup> Pawel M. Kozlowski,<sup>6</sup> Kevin J. Kubarych,<sup>1,4</sup> James E. Penner-Hahn,<sup>1,4</sup> and Roseanne J. Sension<sup>1,2,4\*</sup>

<sup>1</sup>Department of Chemistry, University of Michigan, 930 N University Ave. Ann Arbor, Michigan, 48109-1055, U.S.A.

<sup>2</sup>Department of Physics, University of Michigan, 450 Church Street, Ann Arbor, Michigan, 48109-1040, U.S.A.

<sup>3</sup>Linac Coherent Light Source, SLAC National Accelerator Laboratory, 2575 Sand Hill Road, Menlo Park, CA 94025, U.S.A.

<sup>4</sup>Biophysics, University of Michigan, 930 N University Ave. Ann Arbor, Michigan, 48109-1055, U.S.A. <sup>5</sup>Program in Applied Physics, University of Michigan, 450 Church Street, Ann Arbor, Michigan, 48109-1040, U.S.A.

<sup>6</sup>Department of Chemistry, University of Louisville, 2320 South Brook Street, Louisville, Kentucky, 40292, U.S.A.

<sup>\*</sup> Corresponding Author: <a href="mailto:rsension@umich.edu">rsension@umich.edu</a>, 734-763-6074

# **Abstract**

Polarized X-ray absorption near edge structure (XANES) at the Co K-edge and broadband UV-visible transient absorption are used to monitor the sequential evolution of the excited state structure of coenzyme B<sub>12</sub> (adenosylcobalamin) over the first picosecond following excitation. The initial state is characterized by sub 100 fs sequential changes around the central cobalt. These are polarized first in the *y* direction orthogonal to the transition dipole and 50 fs later in the *x* direction along the transition dipole. Expansion of the axial bonds follows on a ca. 200 fs time scale as the molecule moves out of the Franck-Condon active region of the potential energy surface. On the same 200 fs time scale there are electronic changes that result in the loss of stimulated emission and the appearance of a strong absorption at 340 nm. These measurements provide a cobalt-centered movie of the excited molecule as it evolves to the local excited state minimum.

# Introduction

The possibility of molecular 'movies', i.e., the ability to observe structural evolution in real time, has driven the development of new spectroscopic and structural methods. The goal of such studies is to answer the question: how do molecules respond when placed on a new potential energy surface following photoexcitation or other perturbation? Ultrafast UV-Visible and IR spectroscopies allow the monitoring of valence electronic and vibrational changes with exceptional time resolution and sensitivity. The recent development of femtosecond X-ray sources, especially X-ray free electron lasers, has taken molecular 'movies' to a new level of precision and sensitivity. Most measurements to-date have focused on 'snapshots' of local minima or kinetic intermediates. Ultrafast X-ray scattering has the potential to track atomic positions as a function of time. <sup>1-11</sup> Of equal importance, ultrafast X-ray absorption spectroscopy provides the opportunity for element-specific structural measurements at the active sites of a wide range of key systems for photocatalysis, energy-storage, and enzymatic activity. <sup>12-23</sup> Both of these techniques provide the opportunity to move from kinetic 'snapshots' to dynamic molecular 'movies'.

Cobalamins comprise an important class of biological cofactors.  $^{24-29}$  Coenzyme  $B_{12}$  (adenosylcobalamin, AdoCbl, Figure 1) catalyzes radical rearrangement reactions via substrate-induced homolysis of the carbon-cobalt bond. Methylcobalamin (MeCbl), with a methyl group replacing the 5'-deoxyadenosyl group in coenzyme  $B_{12}$ , is the active coenzyme in a wide range of methyl transferase enzymes. Although these enzymatic reactions are ground state reactions, the photochemistry of cobalamins is of increasing relevance. For example, the photochemistry of AdoCbl is vital to the sensing function of the newly discovered photoreceptor, CarH.  $^{30-34}$ 

In addition to their biological function, cobalamins provide a promising platform as lightactivated agents for spatially and temporally controlled delivery of therapeutic agents and as a biocompatible scaffold for CO releasing metal carbonyls,<sup>35-37</sup> since the upper axial ligand can be replaced with a wide variety of chemically or biologically active ligands. The photochemistry and photophysics of cobalamins are determined by seams of intersection between several low-lying electronically excited states.<sup>38-42</sup> The positions of these seams and the pathways for photodissociation or internal conversion vary with axial ligand and with environment.

In the work reported here we have used femtosecond X-ray absorption near edge structure (XANES) measurements at the Co-K edge to probe the initial structural dynamics following excitation of a photoactive alkylcobalamin, coenzyme B<sub>12</sub>. These measurements expand on our previous studies of the dynamics of CNCbl<sup>13,14</sup> by comparing XANES and UV-visible transient absorption measurements. This combination provides unprecedented detail on the initial excited state dynamics, coupling structural dynamics with changes in the excited electronic configuration, and moves beyond the limitations of kinetic models and coherent quasi-harmonic vibrational oscillations.

Figure 1. Coenzyme  $B_{12}$ , (Adenosylcobalamin, AdoCbl). The x, y, and z directions as defined in the text are indicated on the figure. The x-direction is defined by the transition dipole direction excited at 540 nm and approximately connects the two methyl groups on either side of the corrin ring.

#### Methods

# **Experimental Methods**

XANES difference spectra,  $\Delta S(t) = S_{on}(t) - S_{off}$ , were obtained for time delays between -0.5 ps and 1.2 ps using the XPP instrument of the X-ray free electron laser LCLS at SLAC. 43 The AdoCbl sample was dissolved in ultrapure deionized water or ethylene glycol to a concentration of 5 mM and pumped through a glass nozzle to achieve a stable 50 µm diameter jet of solution. The X-ray beam and laser beam travel in a nearly collinear geometry (~1° crossing angle) and were overlapped with the sample about 500 μm below the nozzle. The optical pump pulse (~50 fs full width at half maximum (FWHM)) was centered at 540 nm or 365 nm. The X-ray probe pulse (~40 fs FWHM) was tuned from 7.7 keV to 7.8 keV by using a Si(111) channel cut monochromator (1.4×10<sup>-4</sup> ΔE/E resolution) and cobalt X-ray fluorescence was collected and used as a measure of X-ray absorption where the signal was normalized to a reference I<sub>0</sub>. More details are found elsewhere. 44 The jitter between the X-ray and optical laser was recorded pulse by pulse and used to sort the XANES spectra into finer time steps. The data were averaged using 50 fs bins centered every 25 fs. The combined final instrument response function, including the X-ray and optical laser pulse durations, as well as the jitter measurement error, is estimated to be  $\sim 125$  fs.  $^{43,45}$  The polarization of the optical pulse was rotated between horizontal and vertical to obtain parallel and perpendicularly polarized difference spectra using a remote-controlled optical waveplate. The measured XANES spectrum with the optical laser off is in excellent agreement with the spectrum reported by Champloy et al. for AdoCbl free of radiation damage.<sup>46</sup>

The UV-visible transient absorption measurements were performed using a tunable Ti:sapphire based laser system (Spitfire, Spectra-Physics) in the LUMOS laboratory. The sample

was a thin (ca. 300µm) wire-guided flow to minimize coherent artifacts at short time delays. The excitation wavelength was 575 nm from a noncollinear optical parametric amplifier (TOPAS White, Light Conversion) and the probe was a broadband continuum spanning the range from <330 nm to 750 nm generated by focusing the fundamental at ca. 800 nm into a 5 mm CaF<sub>2</sub> plate. The polarization was alternated between parallel and perpendicular with three scans collected for each polarization. The resulting difference spectra used to calculate the absorption anisotropy,  $r(t) = (\Delta A_{\parallel}(t) - \Delta A_{\perp}(t)) / (\Delta A_{\parallel}(t) + 2\Delta A_{\perp}(t)),$  and the isotropic difference spectrum  $\Delta A_{iso}(t) = \frac{1}{3} (\Delta A_{\parallel}(t) + 2\Delta A_{\perp}(t))$ . Analysis of the optical absorption anisotropy is available in supporting information. An additional data set was collected at magic angle (54.7°) using a 1 mm quartz flow cell and a continuum generated by focusing ca. 400 nm into the CaF<sub>2</sub> plate. Because the continuum extends below 300 nm with significant intensity, this data set provides a better measure of the relative intensity of the excited state γ band between 300 nm and 350 nm. However, the thicker sample and use of a flow cell results in coherent features that complicate the interpretation at time delays <300 fs.

#### Computational methods

The computations reported in this work, geometry optimization and frequency calculations, have been performed using density functional theory (DFT) with the non-hybrid (GGA) Becke-Perdew (BP86) exchange-correlation functional together with TZVP basis set for H atom and TZVPP for Co, C, O and N atoms, respectively as implemented in Gaussian09.<sup>47</sup> The X-ray crystallographic structure of AdoCbl<sup>48</sup> has been used to construct the truncated model, Im-[Co(III)corrin]-Ado<sup>+</sup>. The lower dimethylbenzimidazole base, was replaced by imidazole (Im), while the amide side chains of corrin ring along with the nucleotide loop have been truncated and

replaced with hydrogen atoms. Similar simplified structural models of cobalamins have been successfully used in previous vibrational studies.<sup>49,50</sup> Due to the incomplete treatment of correlation energy and to take into account approximately the effects of anharmonicity, scaling of frequencies was applied.<sup>51,52</sup> To obtain the best agreement with experiment, the DFT-based computed frequencies of Im-[Co(III)corrin]-Ado<sup>+</sup> were uniformly scaled by 0.86.<sup>49,50</sup>

The ground state XANES spectrum was simulated using the truncated Im-[Co(III)corrin]-Ado<sup>+</sup> structure and the FDMNES code.<sup>53,54</sup> The molecule was aligned according to the axis system defined in Figure 1 to allow decomposition of axial and equatorial contributions.

# **Results**

Femtosecond time-resolved X-ray absorption from 7.7 keV to 7.8 keV was measured following excitation of AdoCbl in water and in ethylene glycol at 540 nm. Over the first picosecond the excited state dynamics are independent of solvent. Here we will focus primarily on the data obtained in water. The data obtained in ethylene glycol, which are included in supporting information, are somewhat noisier but are in agreement with the data measured in water. Time-resolved XANES (tr-XANES) data obtained with parallel and perpendicular polarization of the optical and X-ray pulses allows construction of the isotropic tr-XANES difference spectrum and separation of the tr-XANES difference spectrum into contributions polarized parallel (x) and perpendicular (y+z) to the transition dipole direction of the optical transition.<sup>14</sup>

$$\Delta S_{Iso} = \Delta S_{\parallel} + 2\Delta S_{\perp} = \Delta S_{x} + \Delta S_{y+z}$$

$$\Delta S_{x} = 2\Delta S_{\parallel} - \Delta S_{\perp}$$

$$\Delta S_{y+z} = 3\Delta S_{\perp} - \Delta S_{\parallel}$$
(1)

The isotropic fs tr-XANES difference spectrum obtained following excitation of AdoCbl at 540

nm is plotted in Figure 2(a). The dominant features are (1) a prompt bleach of the 1s→3d pre-edge transition at 7.711 keV, (2) a rapid increase in absorption at 7.729 keV, (3) a delayed increase in absorption at 7.721 keV correlated with an overall red-shift of the XANES edge, and (4) a delayed absorption feature in the pre-edge region at 7.7085 keV. Additional changes are observed in the higher energy features (see Figure S1). The data obtained in ethylene glycol are similar (Figure S2).

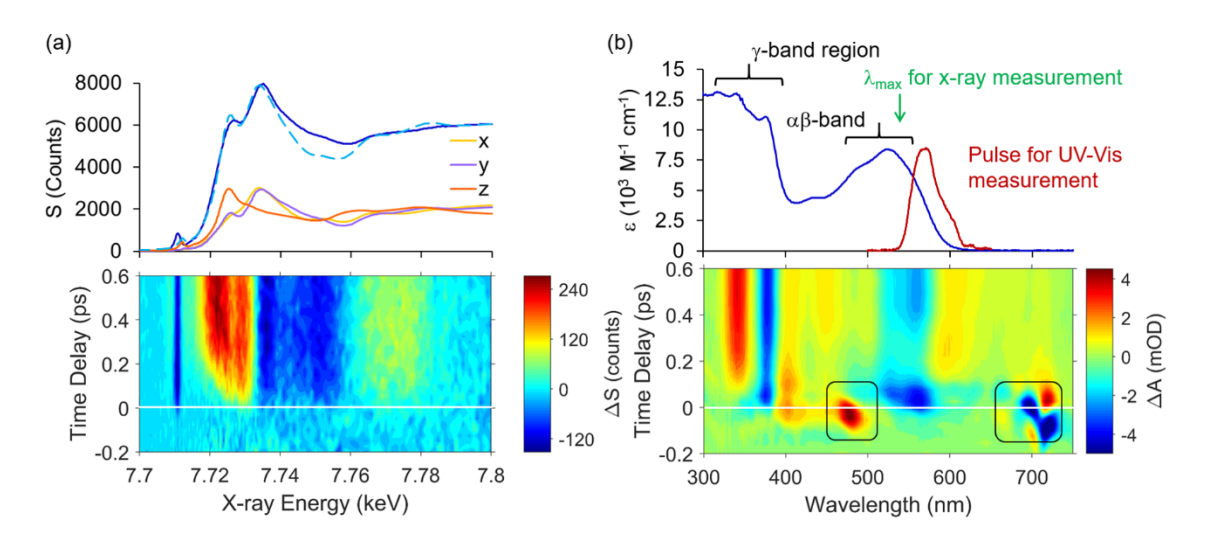


Figure 2. (a) Top: Laser-off XANES spectrum of AdoCbl in water (solid blue) compared with the simulated XANES spectrum (dashed cyan). The decomposition of the simulated spectrum into contributions polarized along the x, y, and z coordinates is also plotted. Bottom: Surface plot of the isotropic XANES difference spectrum from -0.2 ps to 0.6 ps. (b) Top: UV-Visible spectrum of AdoCbl in water. The  $\alpha\beta$ -band is the lowest  $\pi\pi^*$  excitation of the corrin ring. The  $\gamma$ -band region is dominated by contribution from higher energy  $\pi\pi^*$  transitions of the corrin ring. 42,55,56 The excitation pulse for UV-Visible transient absorption and the central wavelength for X-ray transient absorption are indicated. Bottom: Surface plot of the isotropic transient difference spectrum from -0.2 ps to 0.6 ps. The black boxes indicate regions dominated by Stokes and anti-Stokes stimulated Raman scattering from the water solvent.

The fs tr-XANES spectra are compared with broadband transient absorption measurements in

the UV-visible region of the spectrum in Figure 2b. Consistent with the XANES measurement, these data are characterized by an initial transient evolving on a ca. 200 fs time scale. The strong features around 480 nm and 720 nm arise from stimulated Raman scattering in the water solvent. The remaining features are characteristic of the AdoCbl excited state evolution. The initial excited state is characterized by a bleach at 377 nm, an increased absorption at 400 nm, a strong bleach of the visible absorption between 500 nm and 590 nm, and the contribution of a stimulated emission signal to the red of the ground state absorption, 590 nm  $\leq \lambda \leq$  650 nm evidenced by the apparent negative absorption change in this region to the red of the ground state absorption. These features disappear within 200 fs, replaced by a strong  $\gamma$ -band absorption at 340 nm, a weak, but increasing, ground state bleaching signal around 550 nm, and a weak, broad, absorption tail at wavelengths greater than 590 nm.

Difference spectra at selected time delays and time traces at selected energies are plotted in Figure 3. Optical excitation results in a prompt electronic change in the  $\pi$  orbitals of the corrin ring and may include some involvement of Co d orbitals.  $^{38,42}$  The earliest change observed in the X-ray absorption spectrum is the decrease in absorption of the sharp  $1s \rightarrow 3d$  transition at 7.711 keV. The bleach of this signal appears on a time scale that is consistent with the temporal width and overlap of the X-ray and optical pulses at the sample. The instrument response function (*IRF*) was approximated as a Gaussian function  $IRF(t,\sigma,\delta t) = \frac{1}{\sigma\sqrt{2\pi}}e^{-\frac{1}{2}(\frac{t-\delta t}{\sigma})^2}$  with FWHM of  $\Delta t = \sigma 2\sqrt{2 \ln 2} = 125$  fs. Every other change in the XANES spectrum is delayed in time from this initial electronic signature; these delayed changes thus report on structural and/or electronic evolution in the excited electronic state following excitation. The fit to the transient at 7.711 keV is used to define t=0 overlap for the tr-XANES data. The UV-visible data in Figure 3(b) is

corrected for dispersion (i.e., chirp) of the broadband continuum using a polynomial function.<sup>57</sup> These data have an IRF of  $\Delta t = 100$  fs, limited by the intrinsic temporal width of the continuum probe generated in 5 mm CaF<sub>2</sub>. The excitation pulse is somewhat shorter than the probe, with an estimated width of <70 fs FWHM.

The isotropic difference spectrum can be used to reconstruct the excited state XANES spectrum as a function of time. Given an excitation percentage,  $\beta$ , the excited state spectrum as a function of time is reconstructed from the isotropic difference spectrum and the measured laser-off spectrum according to:

$$S(t) = \frac{1}{\beta} \left( S_{laser-on}(t) - S_{laser-off} + \beta S_{laser-off} \right)$$
 (2)

For the XANES measurements reported here  $\beta \approx 0.23$ , limited on the low end to  $\beta \geq 0.17$  by the requirement of positive excited state X-ray absorption at all X-ray energies and on the upper end to  $\beta \leq 0.3$  by the magnitude of the cob(II)alamin difference spectrum at long time delays. <sup>12,46,58</sup> At the earliest times the integration of the instrument response function is also included in the value of  $\beta$  to account for the time-dependence of the build-up of excited state population:  $\beta = 0.23 \int_{-\infty}^{t} IRF(t')dt'$ .

The evolution of the reconstructed excited state XANES spectrum is plotted in Figure 3(a). The excited state spectrum is characterized by a rapid increase in intensity between 7.725 keV and 7.730 keV accompanied by a red-shift of the peak at 7.735 keV followed by a slower red-shift of the XANES edge. The excited state UV-visible transient spectra plotted in Figure 3(b) are calculated in the same manner, although the excited fraction is much lower, ca. 3% as estimated from the sample concentration and the magnitude of the signal. The relative intensity between 300 nm and 340 nm at the edge of the broadband continuum generated using 800 nm pulses in CaF<sub>2</sub> is

underestimated in the transient absorption measurements. Estimated spectra at 0.4 ps and 1 ps obtained with a UV continuum generated using 400 nm pulses in  $CaF_2$  are also plotted in Figure 3(b) to illustrate the actual intensity of the excited state  $\gamma$ -band at 340 nm. These data were obtained using a quartz flow cell where coherent artifacts obscure the AdoCbl transient absorption signals for time delays earlier than ca. 0.3 ps.

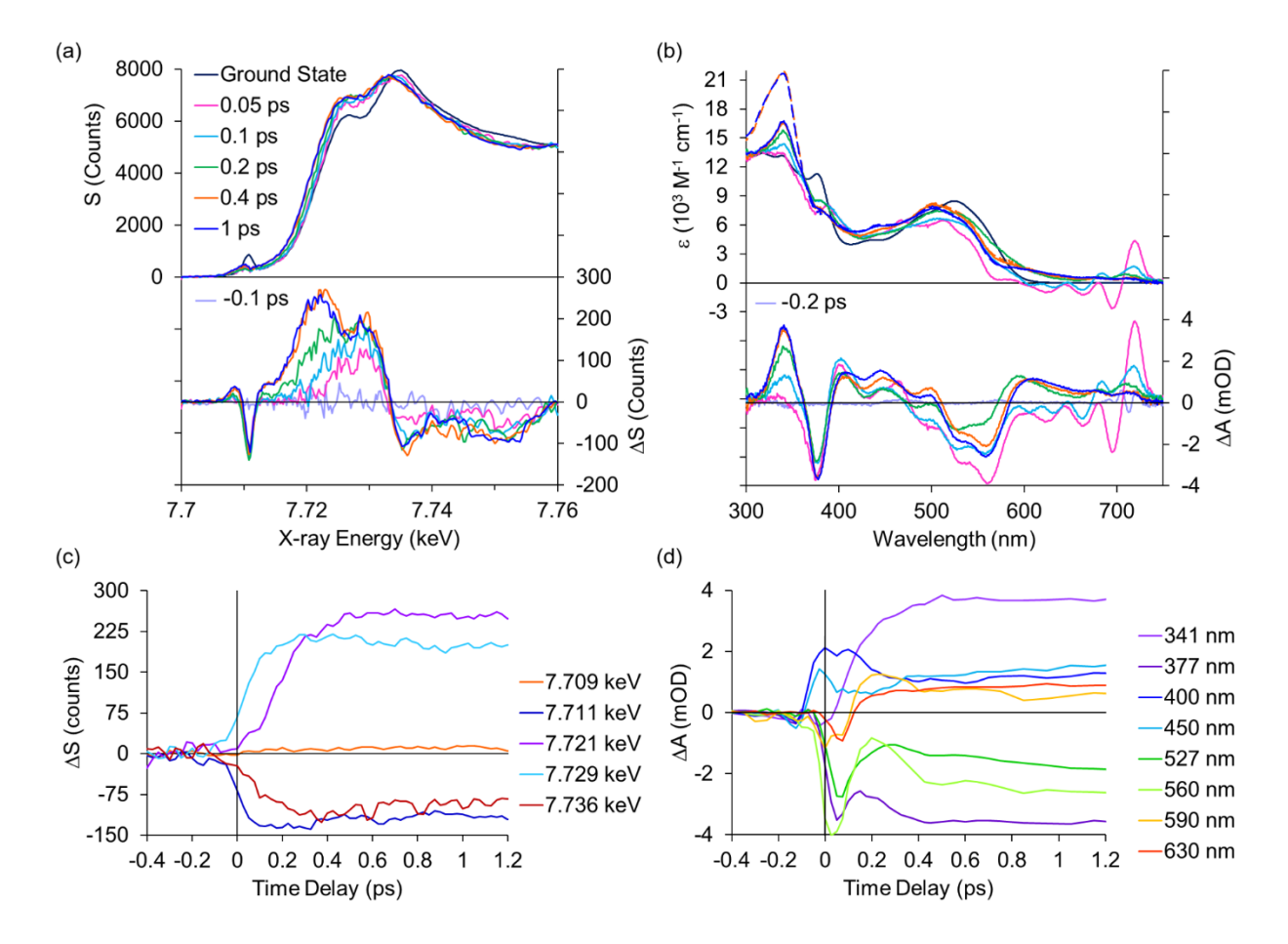


Figure 3. Difference spectra and reconstructed excited state spectra as a function of time. The legend is the same for all plots. (a) XANES spectra in the edge region. The difference spectrum at -0.1 ps illustrates the noise level in the data. (b) UV-visible absorption spectra at the same time delays. The difference spectrum at -0.2 ps illustrates the noise level in the data. The 0.05 ps traces includes remnants of the solvent stimulated Raman scattering contribution. The relative intensity between 300 nm and 340 nm at the edge of the broad band continuum is underestimated. Estimated spectra at 0.4 ps and 1 ps from a separate data set obtained using a deep UV continuum extending below 300 nm are shown for

comparison (dashed lines). (c) Time-dependence at selected X-ray energies. (d) Time dependence at selected UV-visible wavelengths. The signals between 520 nm and 560 nm, including the low frequency oscillatory component at 560 nm, are consistent with single-wavelength high-time-resolution measurements reported earlier.<sup>59</sup>

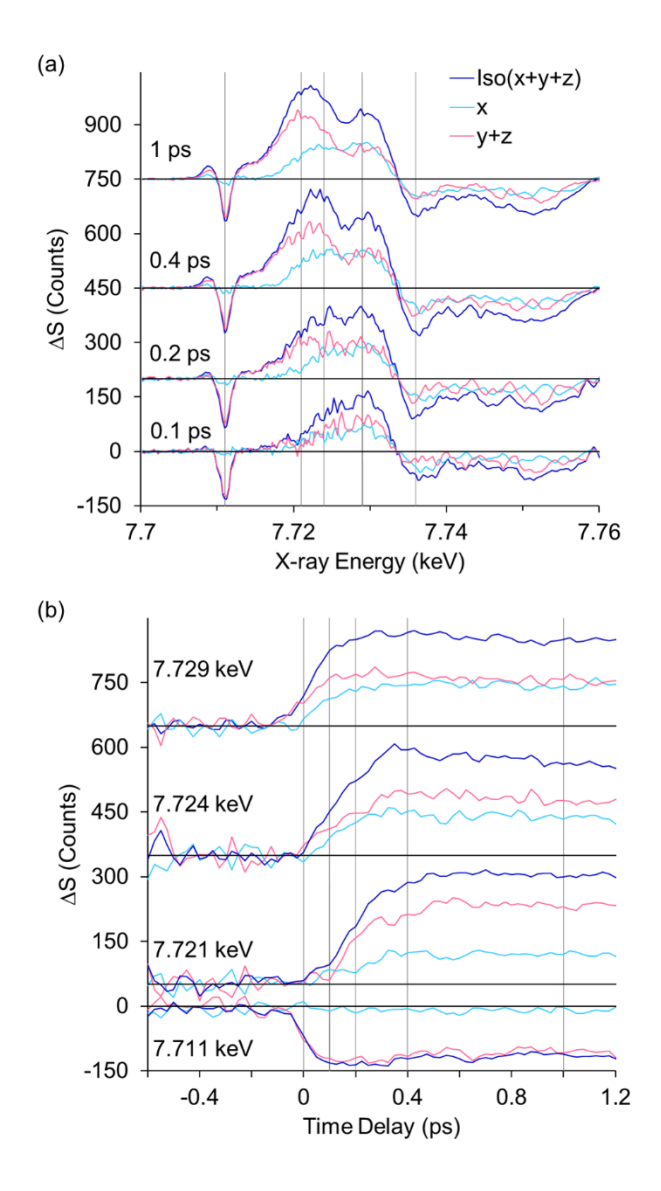


Figure 4. (a) The XANES difference spectrum averaged around four key time delays as indicated on the plot. Both the isotropic spectrum and the decomposition into the x and y+z contributions are plotted. The vertical lines indicate X-ray energies plotted as time traces in (b). (b) Decomposition of the XANES time dependence averaged around five X-ray energies as indicated on the plot into the x and y+z contributions. The legend is the same as in (a). The vertical lines indicate t=0 and the time delays plotted

in (a).

Decomposition of the XANES difference spectrum into x and y+z contributions provides additional insight into the structural dynamics following excitation. Signals at key time delays and X-ray energies are plotted in Figure 4. As noted above, the earliest transient is the bleach of the pre-edge transition at 7.711 keV. The initial bleach is absent in the x component, although a small contribution grows in with time. Of particular interest, the growth of the x and y+z difference signals at 7.729 keV are not simultaneous. The growth of the x-polarized signal is delayed by ca. 50 fs from the y+z signal as shown in Figure 4b. This delay suggests that there are sequential asymmetric changes in the corrin ring over the first 100 fs as discussed in more detail below. Although the data obtained in ethylene glycol solvent are noisier than those in water, the general features are similar: the prompt bleach of the pre-edge transition, the ca. 200 fs delay of the redshift of the XANES edge, and the 50 fs time delay of the x-component with respect to y+z at 7.729 eV are all reproduced (Figure S3).

# **Discussion**

The y and z contributions to XANES can be separated by comparing the effects of UV and visible excitation.

Although it is not possible to associate X-ray absorption intensity at a particular energy with individual atomic positions (see e.g., Fig. 8 of Rossi *et al.* for an illustration of the complexity of XANES data in macrocyclic ligands)<sup>60</sup>, the availability of polarization dependent difference spectra allow us to connect different energy regions with different structural features. Specifically, the y and z components of the difference spectra can be further identified and separated at some X-ray energies by using polarization resolved data obtained at 12 ps in ethylene glycol. By

measuring transient X-ray absorption spectra for both 540 nm excitation, where the transition dipole is defined as "x", and 365 nm excitation, where the transition dipole is approximately orthogonal to x in the corrin ring (i.e.  $\sim$  "y"), it is possible to completely define the transient absorption tensor. The excited state XANES spectrum, and thus the excited state structure, does not change significantly between 1 ps and 12 ps in ethylene glycol (Figure S4). The isotropic difference spectrum in ethylene glycol depends slightly on excitation wavelength, but the general trends are the same following both 540 nm and 365 nm excitation.

As shown in Figure 5,  $\Delta S_x(540 \text{ nm})$  and  $\Delta S_{x+z}(365 \text{ nm})$  are similar from 7.725 keV to 7.733 keV. The same is true when comparing  $\Delta S_{y+z}(540 \text{ nm})$  and  $\Delta S_y(365 \text{ nm})$  over this region. The comparison demonstrates that contributions from x and y dominate in this region with little or no contribution from z. This is consistent with our simulations of the excited state structure of MeCbl, where we found that the increase in X-ray absorption around 7.729 keV arises from expansion and distortion of the corrin ring contributing primarily to the x- and y-polarized difference spectra. Changes in  $\Delta S_z$  dominate from 7.711 keV to 7.717 keV with little or no contribution from either  $\Delta S_x$  or  $\Delta S_y$ . From 7.718 keV to 7.723 keV all three components make a significant contribution to the difference signal, although it is clear that  $\Delta S_z$  makes the major contribution to the red-shift of the XANES edge.

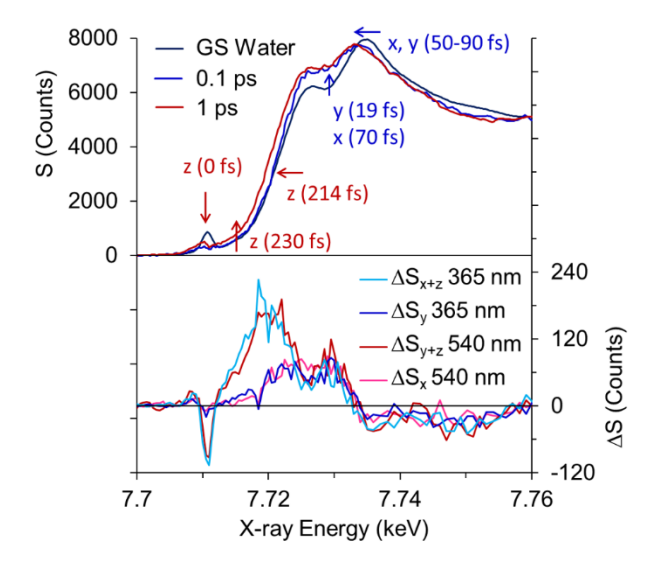


Figure 5. Top: Identification of the changes in the XANES spectrum following excitation of AdoCbl at 540 nm. The labels indicate the polarization and approximate time delays. Bottom: Decomposition of the difference spectrum 12 ps following excitation of AdoCbl in ethylene glycol (EG) at 540 nm and 365 nm.

# Time dependent changes in the XANES provide evidence for sequential structural changes.

Although it is possible to fit the early time data to a sum of exponential components, such a fit provides little physical insight into the excited state dynamics. The early dynamics are not expected to obey kinetic rate equations giving rise to exponential population evolution. Rather, wave packet motion on the excited state surface evolves toward the excited state local minimum energy structure on a time scale of a few hundred femtoseconds accompanied by changes in the electronic configuration. Assuming that the dynamics are well described as ballistic wave packet motion on the excited state surface, the rise in the X-ray signal can be fit using a step function  $H(t,\delta t)$  convoluted with a Gaussian to give the empirical lineshape  $F(t,\sigma_f,\delta t) = H(t,\delta t)*G(t,\sigma_f)$ ,

$$F(t, \sigma_f, \delta t) = \int_{-\infty}^{t} \frac{1}{\sigma_f \sqrt{2\pi}} e^{-\frac{1}{2} \left(\frac{x - \delta t}{\sigma_f}\right)^2} dx, \text{ where } \sigma_f \text{ is the effective rise time of the X-ray signal at that}$$

energy and  $\delta t$  is the delay in the changes relative to the changes at 7.711 keV. A small exponential

decay component is included with the step function where necessary (e.g. 7.711 keV). Because both the X-ray and optical pulses have a finite width the effective rise time,  $\sigma_f$ , is approximately the convolution of the *IRF* with the broadening due to the intrinsic rate of molecular response  $\sigma_m$ . Assuming that both the *IRF* and the molecular response are Gaussian, then  $\sigma_f \approx \sqrt{\sigma_{IRF}^2 + \sigma_m^2}$ . This allows an estimate of the intrinsic molecular response  $\sigma_m$  from  $\sigma_f$  and  $\sigma_{IRF}$  (See SI for additional details). While the fitted parameters  $\delta t$  and  $\sigma_m$  do not necessarily represent specific molecular motions, they provide a convenient way to characterize the energy dependent changes in the XANES spectrum and at specific energies may be assigned to qualitative molecular changes.

Table 1. Fits of select time-traces following excitation of AdoCbl in water to a step function delayed by  $\delta t$  and convoluted with a Gaussian rise of width  $\sigma_f$ . The final two columns,  $\sigma_m$  and  $\Delta t_m$  represent the width of the rise after deconvolution of the *IRF*. Fits at additional energies are provided in Table S1.

X-ray energy	Component <sup>b</sup>	$\delta t$ (fs)	$\sigma_f(fs)$	$\sigma_m$ (fs)	$\Delta t_m = \sigma_m  2\sqrt{2 \ln 2}$
(keV)					(FWHM, fs)
$7.711^{a}$	<i>y</i> + <i>z</i> ( <i>z</i> )	0	53 (σ <sub>IRF</sub> )	0	0
7.736	<i>x</i> + <i>y</i> + <i>z</i>	93	115	102	241
7.729	$\boldsymbol{x}$	70	79	59	139
7.729	y+z(y)	19	85	67	157
7.721	X	182	126	114	269
7.721	y+z	195	108	94	222
7.720	$\boldsymbol{x}$	199	115	102	241
7.720	y+z	223	129	118	277
7.715	y+z	232	102	87	204
7.714	y+z	227	96	80	189
7.709	x+y+z	196	221	214	504

<sup>&</sup>lt;sup>a.</sup> The values obtained in the fit to the 7.711 keV trace are used to define t=0 and the width of the instrument response function. Every other change is later and slower.

<sup>&</sup>lt;sup>b.</sup> Experimental difference spectra that were fit to determine  $\delta t$  and  $\sigma_f$ . For 7.711 keV and 7.729 keV, independent data measured following 365 nm illumination demonstrates that the observed change is primarily polarized along the z or y axis respectively (see text).

Fits to the X-ray absorption at key energies are summarized in Table 1 with additional energies reported in Table S1. Time traces at 7.729 keV characterize the rapid increase in absorption between 7.725 keV and 7.730 keV. At this energy the y+z component is delayed by ca.  $\delta t = 19$  fs, with an intrinsic Gaussian rise of  $\Delta t_m = 157$  fs. As demonstrated above, this signal is dominated by the y-component with minimal contribution from z. The x component displays a slightly sharper rise (ca. 139 fs) but is delayed by 70 fs. Near the XANES peak at 7.735 keV the x and y+z (y) contributions are similar. The isotropic absorption increase at 7.731 keV is delayed by 50 fs while the bleach at 7.736 keV develops slightly later, delayed by 90 fs from t=0; both of these signals have a longer Gaussian rise >200 fs. These signals report on the sequential and asymmetric distortion of the corrin ring around the central Co atom at the very earliest times following optical excitation.

The shift of the red-edge of the XANES spectrum, monitored using the y+z component between 7.716 keV and 7.721 keV (Figure 5), is characterized by a Gaussian rise (247 fs  $\pm$  44 fs) delayed by 214 fs  $\pm$  15 fs from time zero. The error bars represent the standard deviation of the values obtained in fits to the traces plotted in Figure 6. The parameters for the individual fits are reported in Table S1. This transient signal in this region is dominated by changes in the axial z-polarized direction and reports on the elongation of one or both axial bonds following photoexcitation. The axial elongation is delayed from excitation by ca. 214 fs and ballistic with a rise time of ca. 250 fs. The x component at the edge (7.719-7.721 keV, not shown in Figure 6) appears slightly earlier,  $197 \pm 14$  fs with a ca. 270 fs Gaussian rise, but significantly later than the absorption increase between 7.725 and 7.730 keV.

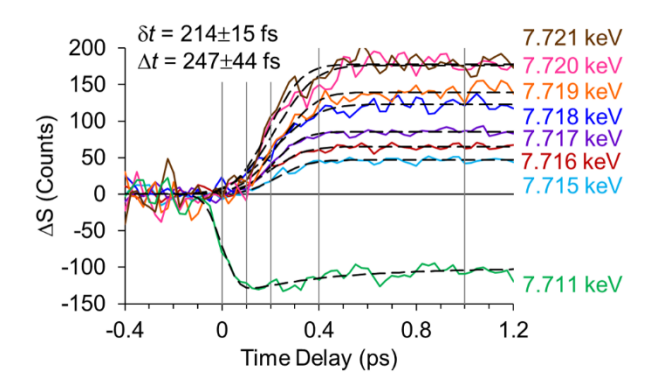


Figure 6. Fits of the y+z data at the peak of the initial pre-edge bleach and along the red edge of the XANES spectrum illustrating the delayed shift of the z-polarized edge. The dashed lines represent the fits to the data. The light vertical lines are the same as in Figure 4b. The average values and standard deviation of  $\delta t$  and  $\Delta t_m$  from 7.721 keV to 7.715 keV are given on the plot.

Finally, the differences in the pre-edge region report on changes in the electronic configuration as a function of time-delay through Co 1s excitation to bound valence orbitals. The y+z absorption at 7.714 and 7.715 keV is delayed slightly from the red-shift of the XANES edge, following the 7.711 keV bleach by 230 fs, with a ca. 200 fs Gaussian rise. There is no significant x component between 7.711 keV and 7.717 keV. The pre-edge absorption at 7.709 keV includes both x and y+z contributions. Although the small size of the signal at 7.709 keV precludes separate analysis of the x and y+z components, the isotropic x+y+z signal at 7.709 keV is noticeably delayed (~196 fs) from t=0 and is characterized by a very broad, ca. 500 fs, integrated Gaussian rise. This suggests a change in the electronic configuration giving rise to intensity in Co 1s $\rightarrow$ 3d transitions with x, y, and z-polarized contributions.

# Time-resolved differences in UV-visible and XANES reveal coupled changes in electronic and atomic structure.

The dominant electronic change following excitation of AdoCbl at 540 nm is often described as involving the depopulation of a corrin- $\pi$  orbital and the population of a corrin- $\pi$ \* orbital. The

observation that there is a bleach of the *z*-polarized pre-edge transition at 7.711 keV, typically described as a 1s-3d transition, on a time-scale that matches the  $\pi$ - $\pi$ \* excitation is thus surprising, since this seems to suggest that the initial excitation involves an increase in electron density in the cobalt- $\sigma$ \* 3d orbitals. Resolution of this apparent discrepancy begins with recognition that TD-DFT calculations predict some amount of Co  $3d_{xz}$ ,  $3d_{yz}$ , and  $3d_z$ 2 character in the " $\pi$ \*" HOMO, but more nearly pure corrin  $\pi$ \* character for the excited state. Similarly, the "1s-3d" transition in fact represents excitation from the 1s core level into a molecular orbital with significant 3d character. The observed 1s-3d transition in AdoCbl is unusually intense in comparison with other 6-coordinate Co(III) complexes; 46.61 this is attributable to a small amount of Co 3d + 4p mixing, which provides some dipole character to the otherwise dipole-forbidden 1s-3d transition. The observed bleaching in *z* may thus represent a small decrease in the Co 4p<sub>z</sub> character of the nominally  $3d_z$ 2 molecular orbital.

The  $\pi\to\pi^*$  excitation of the corrin ring initiates subsequent structural changes in the AdoCbl molecule. The first change, ca. 19 fs after excitation, is in the y direction, perpendicular to the transition moment excited in the corrin ring, resulting in an increase in the X-ray absorption between 7.725 keV and 7.73 keV. This is followed in  $\sim$  50 fs by a similar change in the x direction, along the transition dipole initially excited, between 7.725 keV and 7.73 keV accompanied by a red-shift of the xy polarized peak at 7.735 keV. These signals report primarily on deformations in the corrin ring arising from  $\pi\to\pi^*$  excitation. During this initial phase, a stimulated emission signal is observed in the UV-visible transient absorption spectra for 590 nm  $\leq \lambda \leq$  650 nm indicating evolution on the optically bright electronic state.

Elongation of the axial bonds follows ring expansion ca. 200 fs after excitation, resulting in red-shift of the z-polarized XANES edge and the abrupt loss of the stimulated emission

contribution to the UV-Visible transient spectrum as the molecule moves out of the region that is optically coupled to the ground state (Figure 7). There is also a much smaller shift in the x and presumably y-polarized contributions to the XANES edge. As the axial bonds change, a strong  $\gamma$ -band absorption appears at 340 nm in the UV-visible spectrum accompanied by a blue-shift of the  $\alpha\beta$ -band absorption. The UV-visible spectrum of this excited state is similar in structure to the spectrum observed for MeCbl, although the blue-shift of the  $\alpha\beta$ -band absorption is larger (Figure S6). $^{62-64}$ 

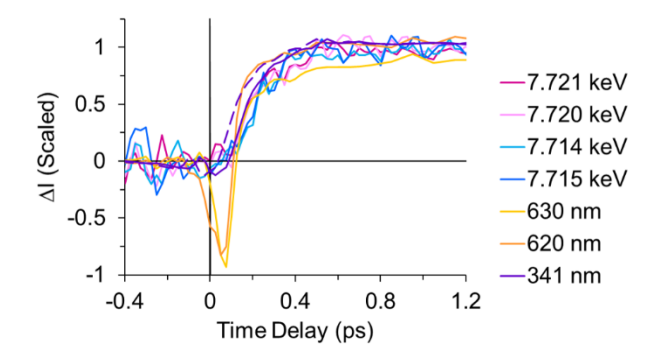


Figure 7. Comparison of the time dependence in the X-ray and UV transients. The y+z signal arising from the red-shift of the XANES edge is compared with the disappearance of stimulated emission (630 nm and 620 nm) and the appearance of the excited state  $\gamma$ -band (340 nm). Precise assignment of t = 0 in the UV is uncertain and the appearance of the  $\gamma$ -band either precedes by ca. 50 fs (dashed line) or accompanies (solid line) the red-shift of the XANES edge. See Figure S5 for a similar plot in ethylene glycol.

The excited state that is formed within a few hundred femtoseconds of excitation of AdoCbl in both water and ethylene glycol, as well as the one that is probed at 100 ps following excitation of MeCbl, are typically described as a metal-to-ligand charge transfer (MLCT) although a more precise description might be as a  $\sigma$ -bond-ligand charge transfer state (SBLCT), in which electron density has moved from axial Co-ligand bonding molecular orbitals to corrin  $\pi^*$  orbitals.<sup>65</sup> Recent

TD-DFT calculations of AdoCbl predict that the electronic configuration is  $d_{xz}/d_z^2 + \pi \rightarrow \pi^*$ . The relaxed  $S_1$  AdoCbl excited state calculated using TD-DFT is characterized by an expansion of the Co-C bond by 0.046 Å (~2.3%) and contraction of the Co-N<sub>DMB</sub> bond 0.147 Å (~6.7%) resulting in a net decrease in the average axial distance to the Co. The predicted expansion of the Co-C bond in AdoCbl is qualitatively consistent with the experimental XANES difference spectra, but the large contraction of the Co-N<sub>DMB</sub> bond is inconsistent with the experimental results. A similar contraction of the Co-N<sub>DMB</sub> distance was predicted for MeCbl; 66 in that case as well the tr-XANES suggest that the experimental contraction in Co-N<sub>DMB</sub> is smaller than predicted. It may be that the absence of the full dimethylbenzimidazole group and the tether to the corrin ring in the reduced model used for TD-DFT calculations results in an over-estimate for the contraction of the lower bond. Specific interactions with the solvent may also play a role. A more detailed analysis of the structural changes following excitation will require systematic simulation of the excited state XANES for a range of plausible AdoCbl structures along excited state trajectories.

Both optical and X-ray differences show evidence for low frequency coherent vibrational oscillations.

In addition to the loss of stimulated emission and appearance of the excited state γ-band, there is evidence of a small amplitude oscillation in the transient absorption signals between 550 nm and 600 nm (Figure 3d). A similar oscillation is seen in the XAS pre-edge bleach at 7.711 keV and in the XANES edge at 7.721 keV (Figure 6). Additional evidence for coherent oscillation may also be present in the higher energy XANES region, but the signal to noise ratio of the current data is insufficient for further analysis in this region (see Figure S8). The visible transient absorption data are consistent with single wavelength high time resolution measurements reported earlier.<sup>59</sup> The residual oscillatory components in the visible and X-ray regions of the spectrum are compared in

Figure 8 and may arise from wave packet evolution on the ground or excited state potential energy surfaces following impulsive excitation. The period is approximately 390 fs corresponding to one or more vibrations around 85 cm<sup>-1</sup>, a frequency range difficult to measure using standard vibrational methods. The appearance of this oscillation in the bleach of the Co 1s $\rightarrow$ 3d<sub>z</sub><sup>2</sup> pre-edge transition suggests that the motion is coupled to the mixing of the Co 4p<sub>z</sub> and 3d<sub>z</sub><sup>2</sup> orbitals. The out-of-phase oscillations in *x* and *y*+*z* at the peak of the edge shift (7.721 keV) suggest a ring deformation, a torsion, or a wag of the Co-C or Co-N<sub>DMB</sub> bonds modulating projections on *x* as well as on *y* and/or *z*.

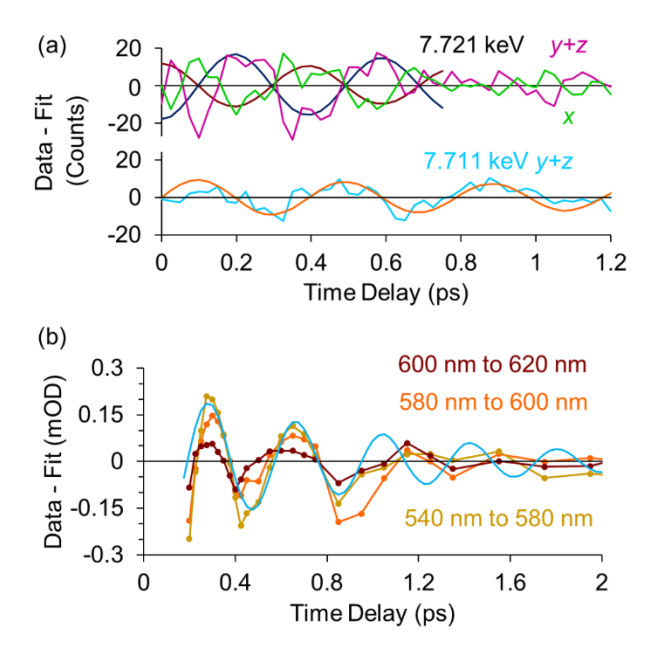


Figure 8. (a) X-ray difference signal residual oscillatory component at 7.711 keV and averaged from 7.72 to 7.7215 keV (labeled 7.721 keV). The residuals at 7.711 keV are compared with a sine wave,  $\sin(\omega t)$  where  $\omega = 16$  rad/ps corresponding to an 85 cm<sup>-1</sup> vibration. At 7.721 keV the frequency is the same but there is a phase shift of  $\pi/2$  resulting in a cosine wave and the oscillation is only apparent for the first 800 fs. (b) Visible difference signal residual oscillatory signals averaged over the given wavelength ranges. The residuals are compared with a sine wave where  $\omega = 16.5$  rad/ps corresponding to 87.5 cm<sup>-1</sup>. The frequency may decrease slightly with time delay. See Figure S9 for a plot comparing

the signals, fits, and residuals.

Given our conclusion (e.g., Figure 5) that absorbance changes at 7.721 keV are primarily due to changes in the axial ligands, it is, at first glance, surprising that we see oscillations in the xpolarized absorption at this energy. However, examination of possible normal modes (Table S2) suggests an explanation. DFT calculations of the AdoCbl vibrational modes identify a Co-N<sub>IM</sub> stretch,  $v_{15}$ , at ~87 cm<sup>-1</sup> and a wag of the Co-C bond,  $v_{16}$ , at ~92 cm<sup>-1</sup> (see Figure 9). One or both of these modes, which involve motion of the axial ligands and corrin ring, are good candidates for the observed oscillation. In particular the  $v_{16}$  Co-C wag with projections of the axial bonds on the x and y axes could account for the out of phase oscillations in the x and y+z signals at 7.721 keV, where the data are the most sensitive to changes in the axial bond lengths. The oscillatory component is also consistent with previous observations of doming and ruffling in hemes and may include response of the corrin ring to changes in the axial bonding. <sup>21,67-69</sup> Modes with significant ring doming motions are calculated at 74 cm<sup>-1</sup> and 106 cm<sup>-1</sup> ( $v_{13}$  and  $v_{18}$ , Figure S10). While  $v_{13}$ does not modulate the axial bonds significantly, and  $v_{18}$  modulates the Co-N<sub>IM</sub> projection on z and both Co-N<sub>IM</sub> and Co-C projections on y and may contribute to the observations. Precise assignment of the motions involved in each probe region will require more extensive data sets and detailed simulations including other motions of the corrin ring and multiscattering simulations of the XANES region. Nevertheless this work shows great promise for the ability to resolve coherently driven atomic motion even for a large macrocyclic complex using transient X-ray spectroscopy. There is reason to be optimistic that transient X-ray absorption with its structural sensitivity will be definitive in its ability to assign the coherent motion to specific potential energy surfaces, which can be important for unraveling photochemical mechanism, but challenging or impossible in optical spectroscopy.<sup>23,70-72</sup>

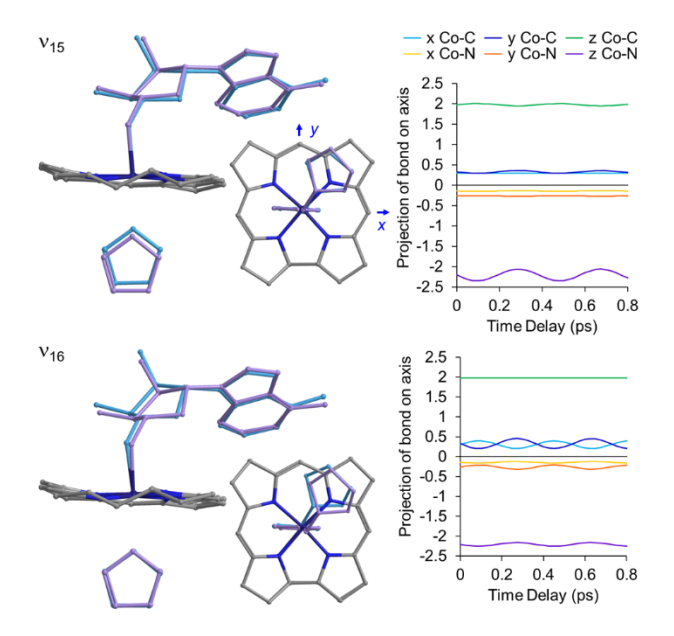


Figure 9. Positive (violet) and negative (blue) extrema using the calculated eigenvector displacements for  $\nu_{15}$  and  $\nu_{16}$ . The plots to the right compare the projection of the Co-C and Co-N<sub>IM</sub> bonds on the molecule-fixed x, y and z axes for each vibrational mode. See Figure S10 for other nearby modes.

# **Conclusions**

Femtosecond time-resolved XANES and UV-Visible measurements of excited state dynamics following excitation of AdoCbl in water and in ethylene glycol in the visible  $\alpha\beta$  band demonstrate rapid sequential distortion of the corrin ring of the molecule in the initial optically bright state. Expansion of one or both axial bonds follows on a ca. 214 fs time scale as the molecule moves out of the Franck-Condon active region of the potential energy surface. Electronic changes resulting in a change of the UV-visible spectrum, most notably the appearance of a strong  $\gamma$ -band absorption at 340 nm, accompany the structural changes revealed in the XANES spectrum. The side-by-side comparison of the optical transient absorption spectrum and the XANES difference spectrum is able to identify the nuclear response in the bright state and the changes correlated with evolution out of this state. The asymmetric responses report on the sequential nature of wavepacket evolution

in the excited state of AdoCbl.

Previous studies on CNCbl demonstrated a ballistic expansion to a maximum at 190 fs followed by a contraction to the excited state minimum within 500 fs. For AdoCbl, the response of the axial nuclei is slower, reaching a maximum between 400 and 500 fs. This may be due to the more massive adenosyl ligand. However, the shape of the excited state potentials are modulated by the different axial ligands of cobalamin compounds and this is likely the more important factor. 38,41

As with many other molecular systems, a coherent vibrational oscillation is apparent in the optical transient absorption measurement. Here, an oscillation is observed in both the optical and the X-ray measurements. This vibrational coherence highlights the importance of one or more previously uncharacterized low frequency modes in the optical excitation of AdoCbl.

The optical and X-ray measurements reported here provide a cobalt-centered movie of the electronically excited molecule as it evolves to the local excited state minimum.

# Acknowledgements

This work was supported by grants from the National Science Foundation NSF-CHE 1464584, NSF-CHE 1836435 to RJS; NSF-CHE 1565795 to KJK. Portions of this work were carried out in the Laboratory for Ultrafast Multidimensional Optical Spectroscopy (LUMOS), supported by NSF-CHE 1428479. Use of the Linac Coherent Light Source (LCLS), SLAC National Accelerator Laboratory, is supported by the U.S. Department of Energy, Office of Science, Office of Basic Energy Sciences under Contract No. DE-AC02-76SF00515.

# **Supporting Information**

Plots of transient optical and X-ray spectra in ethylene glycol, comparison of MeCbl and AdoCbl excited states, extended discussion of fits to the XANES data, plots showing oscillatory component and vibrational modes, table of low frequency vibrations, optical absorption anisotropy in water.

# References

- (1) Ruddock, J. M.; Zotev, N.; Stankus, B.; Yong, H. W.; Bellshaw, D.; Boutet, S.; Lane, T. J.; Liang, M. N.; Carbajo, S.; Du, W. P.; et al. Simplicity beneath complexity: Counting molecular electrons reveals transients and kinetics of photodissociation reactions. *Angew. Chem., Int. Ed.* **2019**, *58*, 6371-6375.
- (2) Kirrander, A.; Weber, P. M. Fundamental limits on spatial resolution in ultrafast X-ray diffraction. *Appl. Sci.* **2017**, *7*, 534.
- (3) Stankus, B.; Budarz, J. M.; Kirrander, A.; Rogers, D.; Robinson, J.; Lane, T. J.; Ratner, D.; Hastings, J.; Minitti, M. P.; Weber, P. M. Femtosecond photodissociation dynamics of 1,4-diiodobenzene by gas-phase X-ray scattering and photoelectron spectroscopy. *Faraday Discuss*. **2016**, *194*, 525-536.
- (4) Budarz, J. M.; Minitti, M. P.; Cofer-Shabica, D. V.; Stankus, B.; Kirrander, A.; Hastings, J. B.; Weber, P. M. Observation of femtosecond molecular dynamics via pump-probe gas phase X-ray scattering. *J. Phys. B* **2016**, *49*, 034001.
- (5) Vester, P.; Zaluzhnyy, I. A.; Kurta, R. P.; Møller, K. B.; Biasin, E.; Haldrup, K.; Nielsen, M. M.; Vartanyants, I. A. Ultrafast structural dynamics of photo-reactions observed by time-resolved X-ray cross-correlation analysis. *Struc. Dyn.* **2019**, *6*, 024301.

- (6) Kong, Q. Y.; Laursen, M. G.; Haldrup, K.; Kjaer, K. S.; Khakhulin, D.; Biasin, E.; van Driel, T. B.; Wulff, M.; Kabanova, V.; Vuilleumier, R.; et al. Initial metal-metal bond breakage detected by fs X-ray scattering in the photolysis of Ru-3(CO)(12) in cyclohexane at 400 nm. *Photochem. Photobiol. Sci.* **2019**, *18*, 319-327.
- (7) Haldrup, K.; Levi, G.; Biasin, E.; Vester, P.; Laursen, M. G.; Beyer, F.; Kjaer, K. S.; van Driel, T. B.; Harlang, T.; Dohn, A. O.; et al. Ultrafast X-ray scattering measurements of coherent structural dynamics on the ground-state potential energy surface of a diplatinum molecule. *Phys Rev Lett* **2019**, *122*, 063001.
- (8) Biasin, E.; van Driel, T. B.; Levi, G.; Laursen, M. G.; Dohn, A. O.; Moltke, A.; Vester, P.; Hansen, F. B. K.; Kjaer, K. S.; Harlang, T.; et al. Anisotropy enhanced X-ray scattering from solvated transition metal complexes. *J. Synchrotron Rad.* **2018**, *25*, 306-315.
- (9) van Driel, T. B.; Kjaer, K. S.; Hartsock, R. W.; Dohn, A. O.; Harlang, T.; Chollet, M.; Christensen, M.; Gawelda, W.; Henriksen, N. E.; Kim, J. G.; et al. Atomistic characterization of the active-site solvation dynamics of a model photocatalyst. *Nat. Commun.* **2016**, *7*, 13678.
- (10) Ki, H.; Oang, K. Y.; Kim, J.; Ihee, H. Ultrafast X-ray crystallography and liquidography. *Annu. Rev. Phys. Chem.* **2017**, *68*, 473-497.
- (11) Stankus, B.; Yong, H. W.; Zotev, N.; Ruddock, J. M.; Bellshaw, D.; Lane, T. J.; Liang, M. N.; Boutet, S.; Carbajo, S.; Robinson, J. S.; et al. Ultrafast X-ray scattering reveals vibrational coherence following Rydberg excitation. *Nat. Chem.* **2019**, *11*, 716-721.
- (12) Michocki, L. B.; Miller, N. A.; Alonso-Mori, R.; Britz, A.; Deb, A.; Glownia, J. M.; Kaneshiro, A. K.; Konar, A.; Meadows, J. H.; Sofferman, D. L.; et al. Probing the excited state of methylcobalamin using polarized time-resolved X-ray absorption spectroscopy. *J. Phys. Chem. B* **2019**, *123*, 6042-6048.

- (13) Miller, N. A.; Deb, A.; Alonso-Mori, R.; Glownia, J. M.; Kiefer, L. M.; Konar, A.; Michocki, L. B.; Sikorski, M.; Sofferman, D. L.; Song, S.; et al. Ultrafast X-ray absorption near edge structure reveals ballistic excited state structural dynamics. *J. Phys. Chem. A* **2018**, *122*, 4963-4971.
- (14) Miller, N. A.; Deb, A.; Alonso-Mori, R.; Garabato, B. D.; Glownia, J. M.; Kiefer, L. M.; Koralek, J.; Sikorski, M.; Spears, K. G.; Wiley, T. E.; et al. Polarized XANES monitors femtosecond structural evolution of photoexcited vitamin B<sub>12</sub>. *J. Am. Chem. Soc.* **2017**, *139*, 1894-1899.
- (15) Kjaer, K. S.; Zhang, W. K.; Alonso-Mori, R.; Bergmann, U.; Chollet, M.; Hadt, R. G.; Hartsock, R. W.; Harlang, T.; Kroll, T.; Kubicek, K.; et al. Ligand manipulation of charge transfer excited state relaxation and spin crossover in Fe(2,2'-Bipyridine)(2)(CN)(2). *Struc. Dyn.* **2017**, *4*, 044030.
- (16) Kjaer, K. S.; Kunnus, K.; Harlang, T. C. B.; Van Driel, T. B.; Ledbetter, K.; Hartsock, R. W.; Reinhard, M. E.; Koroidov, S.; Li, L.; Laursen, M. G.; et al. Solvent control of charge transfer excited state relaxation pathways in [Fe(2,2'-bipyridine)(CN)<sub>4</sub>]<sup>2-</sup>. *Phys. Chem. Chem. Phys.* **2018**, 20, 4238-4249.
- (17) Shelby, M. L.; Lestrange, P. J.; Jackson, N. E.; Haldrup, K.; Mara, M. W.; Stickrath, A. B.; Zhu, D.; Lemke, H. T.; Chollet, M.; Hoffman, B. M.; et al. Ultrafast excited state relaxation of a metalloporphyrin revealed by femtosecond X-ray absorption spectroscopy. *J. Am. Chem. Soc.* **2016**, *138*, 8752-8764.
- (18) Haldrup, K.; Dohn, A. O.; Shelby, M. L.; Mara, M. W.; Stickrath, A. B.; Harpham, M. R.; Huang, J.; Zhang, X.; Møller, K. B.; Chakraborty, A.; et al. Butterfly deformation modes in a photoexcited pyrazolate-bridged Pt complex measured by time-resolved X-ray scattering in

- solution. J. Phys. Chem. A 2016, 120, 7475-7483.
- (19) Chen, L. X.; Shelby, M. L.; Lestrange, P. J.; Jackson, N. E.; Haldrup, K.; Mara, M. W.; Stickrath, A. B.; Zhu, D. L.; Lemke, H.; Chollet, M.; et al. Imaging ultrafast excited state pathways in transition metal complexes by X-ray transient absorption and scattering using X-ray free electron laser source. *Faraday Discuss.* **2016**, *194*, 639-658.
- (20) Chen, L. X.; Zhang, X.; Shelby, M. L. Recent advances on ultrafast X-ray spectroscopy in the chemical sciences. *Chem. Sci.* **2014**, *5*, 4136-4152.
- (21) Levantino, M.; Lemke, H. T.; Schiro, G.; Glownia, M.; Cupane, A.; Cammarata, M. Observing heme doming in myoglobin with femtosecond X-ray absorption spectroscopy. *Struc. Dyn.* **2015**, *2*, 041713.
- (22) Britz, A.; Abraham, B.; Biasin, E.; van Driel, T. B.; Gallo, A.; Garcia-Esparza, A. T.; Glownia, J.; Loukianov, A.; Nelson, S.; Reinhard, M.; et al. Resolving structures of transition metal complex reaction intermediates with femtosecond EXAFS. *Phys. Chem. Chem. Phys.* **2019**, DOI: 10.1039/C1039CP03483H.
- (23) Katayama, T.; Northey, T.; Gawelda, W.; Milne, C. J.; Vanko, G.; Lima, F. A.; Bohinc, R.; Nemeth, Z.; Nozawa, S.; Sato, T.; et al. Tracking multiple components of a nuclear wavepacket in photoexcited Cu(I)-phenanthroline complex using ultrafast X-ray spectroscopy. *Nat. Commun.* **2019**, *10*, 3606.
- (24) Marsh, E. N. G.; Melendez, G. D. R. Adenosylcobalamin enzymes: Theory and experiment begin to converge. *Biochimica Et Biophysica Acta* **2012**, *1824*, 1154-1164.
- (25) Marsh, E. N. G.; Patterson, D. P.; Li, L. Adenosyl radical: Reagent and catalyst in enzyme reactions. *Chembiochem* **2010**, *11*, 604-621.
- (26) Banerjee, R.; Ragsdale, S. W. The many faces of vitamin B<sub>12</sub>: Catalysis by cobalamin-

- dependent enzymes. Annu. Rev. Biochem. 2003, 72, 209-247.
- (27) Bridwell-Rabb, J.; Drennan, C. L. Vitamin B<sub>12</sub> in the spotlight again. *Curr. Opin. Chem. Biol.* **2017**, *37*, 63-70.
- (28) Giedyk, M.; Goliszewska, K.; Gryko, D. Vitamin B<sub>12</sub> catalysed reactions. *Chem. Soc. Rev.* **2015**, *44*, 3391-3404.
- (29) Banerjee, R. Chemistry and Biochemistry of B<sub>12</sub>; John Wiley and Sons: New York, 1999.
- (30) Padmanabhan, S.; Jost, M.; Drennan, C. L.; Elias-Arnanz, M. A new facet of vitamin B<sub>12</sub>: Gene regulation by cobalamin-based photoreceptors. *Annu. Rev. Biochem.* **2017**, *86*, 485-514.
- (31) Kutta, R. J.; Hardman, S. J. O.; Johannissen, L. O.; Bellina, B.; Messiha, H. L.; Ortiz-Guerrero, J. M.; Elias-Arnanz, M.; Padmanabhan, S.; Barran, P.; Scrutton, N. S.; et al. The photochemical mechanism of a B<sub>12</sub>-dependent photoreceptor protein. *Nat. Commun.* **2015**, *6*, 7907.
- (32) Jost, M.; Fernandez-Zapata, J.; Polanco, M. C.; Ortiz-Guerrero, J. M.; Chen, P. Y. T.; Kang, G.; Padmanabhan, S.; Elias-Arnanz, M.; Drennan, C. L. Structural basis for gene regulation by a B<sub>12</sub>-dependent photoreceptor. *Nature* **2015**, *526*, 536-U167.
- (33) Ortiz-Guerrero, J. M.; Polanco, M. C.; Murillo, F. J.; Padmanabhan, S.; Elias-Arnanz, M. Light-dependent gene regulation by a coenzyme B<sub>12</sub>-based photoreceptor. *Proc. Natl. Acad. Sci. U.S.A.* **2011**, *108*, 7565-7570.
- (34) Perez-Marin, M. C.; Padmanabhan, S.; Polanco, M. C.; Murillo, F. J.; Elias-Arnanz, M. Vitamin B<sub>12</sub> partners the CarH repressor to downregulate a photoinducible promoter in Myxococcus xanthus. *Mol. Microbiol.* **2008**, *67*, 804-819.
- (35) Shell, T. A.; Lawrence, D. S. Vitamin B<sub>12</sub>: A tunable, long wavelength, light-responsive platform for launching therapeutic agents. *Acc. Chem. Res.* **2015**, *48*, 2866-2874.
- (36) Shell, T. A.; Shell, J. R.; Rodgers, Z. L.; Lawrence, D. S. Tunable visible and near-IR

- photoactivation of light-responsive compounds by using fluorophores as light-capturing antennas. *Angew. Chem., Int. Ed.* **2014**, *53*, 875-878.
- (37) Santoro, G.; Zlateva, T.; Ruggi, A.; Quaroni, L.; Zobi, F. Synthesis, characterization and cellular location of cytotoxic constitutional organometallic isomers of rhenium delivered on a cyanocobalmin scaffold. *Dalton Trans.* **2015**, *44*, 6999-7008.
- (38) Toda, M. J.; Lodowski, P.; Al Mamun, A.; Jaworska, M.; Kozlowski, P. M. Photolytic properties of the biologically active forms of vitamin B<sub>12</sub>. *Coord. Chem. Rev.* **2019**, *385*, 20-43.
- (39) Lodowski, P.; Toda, M. J.; Ciura, K.; Jaworska, M.; Kozlowski, P. M. Photolytic properties of antivitamins B<sub>12</sub>. *Inorg. Chem.* **2018**, *57*, 7838-7850.
- (40) Ghosh, A. P.; Al Mamun, A.; Lodowski, P.; Jaworska, M.; Kozlowski, P. M. Mechanism of the photo-induced activation of Co-C bond in methylcobalamin-dependent methionine synthase. *J. Photochem. Photobiol. B* **2018**, *189*, 306-317.
- (41) Kozlowski, P. M.; Garabato, B. D.; Lodowski, P.; Jaworska, M. Photolytic properties of cobalamins: A theoretical perspective. *Dalton Trans.* **2016**, *45*, 4457-4470.
- (42) Garabato, B. D.; Lodowski, P.; Jaworska, M.; Kozlowski, P. M. Mechanism of Co-C photodissociation in adenosylcobalamin. *Phys. Chem. Chem. Phys.* **2016**, *18*, 19070-19082.
- (43) Chollet, M.; Alonso-Mori, R.; Cammarata, M.; Damiani, D.; Defever, J.; Delor, J. T.; Feng, Y. P.; Glownia, J. M.; Langton, J. B.; Nelson, S.; et al. The X-ray pump-probe instrument at the Linac Coherent Light Source. *J. Synchrotron Rad.* **2015**, *22*, 503-507.
- (44) Miller, N. A.; Michocki, L. B.; Alonso-Mori, R.; Britz, A.; Deb, A.; Deponte, D. P.; Glownia, J. M.; Kaneshiro, A. K.; Kieninger, C.; Koralek, J.; et al. Antivitamins B<sub>12</sub> in a microdrop: The excited state structure of a precious sample using transient polarized X-ray absorption near edge structure. *J. Phys. Chem. Lett.* **2019**, *10*, 5484-5489.

- (45) Minitti, M. P.; Robinson, J. S.; Coffee, R. N.; Edstrom, S.; Gilevich, S.; Glownia, J. M.; Granados, E.; Hering, P.; Hoffmann, M. C.; Miahnahri, A.; et al. Optical laser systems at the Linac Coherent Light Source. *J. Synchrotron Rad.* **2015**, *22*, 526-531.
- (46) Champloy, F.; Gruber, K.; Jogl, G.; Kratky, C. XAS spectroscopy reveals X-ray-induced photoreduction of free and protein-bound B<sub>12</sub> cofactors. *J. Synchrotron Rad.* **2000**, *7*, 267-273.
- (47) Frisch, M. J.; G. W. Trucks; Schlegel, H. B.; Scuseria, G. E.; Robb, M. A.; Cheeseman, J. R.; Scalmani, G.; Barone, V.; Mennucci, B.; Petersson, G. A.; et al. Gaussian 09; Gaussian, Inc.: Wallingford CT, 2009.
- (48) Ouyang, L.; Rulis, P.; Ching, W. Y.; Nardin, G.; Randaccio, L. Accurate redetermination of the X-ray structure and electronic bonding in adenosylcobalamin. *Inorg. Chem.* **2004**, *43*, 1235-1241.
- (49) Kozlowski, P. M.; Andruniow, T.; Jarzecki, A. A.; Zgierski, M. Z.; Spiro, T. G. DFT analysis of Co-alkyl and Co-adenosyl vibrational modes in B<sub>12</sub>-cofactors. *Inorg. Chem.* **2006**, *45*, 5585-5590.
- (50) Andruniow, T.; Zgierski, M. Z.; Kozlowski, P. M. Vibrational analysis of methylcobalamin. *J. Phys. Chem. A* **2002**, *106*, 1365-1373.
- (51) Kozlowski, P. M.; Jarzecki, A. A.; Pulay, P.; Li, X. Y.; Zgierski, M. Z. Vibrational assignment and definite harmonic force field for porphine. 2. Comparison with nonresonance Raman data. *J. Phys. Chem.* **1996**, *100*, 13985-13992.
- (52) Kozlowski, P. M.; Jarzecki, A. A.; Pulay, P. Vibrational assignment and definite harmonic force field for porphine. 1. Scaled quantum mechanical results and comparison with empirical force field. *J. Phys. Chem.* **1996**, *100*, 7007-7013.
- (53) Bunau, O.; Joly, Y. Self-consistent aspects of X-ray absorption calculations. J. Phys.

- Condens. Matter 2009, 21, 345501.
- (54) Joly, Y. X-ray absorption near-edge structure calculations beyond the muffin-tin approximation. *Phys. Rev. B* **2001**, *63*, 125120.
- (55) Stich, T. A.; Brooks, A. J.; Buan, N. R.; Brunold, T. C. Spectroscopic and computational studies of Co<sup>3+</sup>-corrinoids: Spectral and electronic properties of the B<sub>12</sub> cofactors and biologically relevant precursors. *J. Am. Chem. Soc.* **2003**, *125*, 5897-5914.
- (56) Giannotti, C. In *B12*; Dolphin, D., Ed.; John Wiley and Sons: New York, 1982; Vol. 1, p 393-430.
- (57) Kovalenko, S. A.; Dobryakov, A. L.; Ruthmann, J.; Ernsting, N. P. Femtosecond spectroscopy of condensed phases with chirped supercontinuum probing. *Phys. Rev. A* **1999**, *59*, 2369-2384.
- (58) Cole, A. G.; Yoder, L. M.; Shiang, J. J.; Anderson, N. A.; Walker II, L. A.; Banaszak Holl, M. M.; Sension, R. J. Time-resolved spectroscopic studies of B<sub>12</sub> coenzymes: A comparison of the primary photolysis mechanism in methyl-, ethyl-, n-propyl-, and 5'-deoxyadenosylcobalamin. *J. Am. Chem. Soc.* **2002**, *124*, 434-441.
- (59) Sension, R. J.; Cole, A. G.; Anderson, N. A.; Shiang, J. J. In *Ultrafast Phenomena XII*. *Springer Series in Chemical Physics, vol 66.*; Springer: Berlin, Heidelberg, 2001, p 648-650.
- (60) Rossi, G.; d'Acapito, F.; Amidani, L.; Boscherini, F.; Pedio, M. Local environment of metal ions in phthalocyanines: K-edge X-ray absorption spectra. *Phys. Chem. Chem. Phys.* **2016**, *18*, 23686-23694.
- (61) Schrapers, P.; Mebs, S.; Goetzl, S.; Hennig, S. E.; Dau, H.; Dobbek, H.; Haumann, M. Axial ligation and redox changes at the cobalt ion in cobalamin bound to corrinoid iron-sulfur protein (CoFeSP) or in solution characterized by XAS and DFT. *Plos One* **2016**, *11*, e0158681.

- (62) Harris, D. A.; Stickrath, A. B.; Carroll, E. C.; Sension, R. J. Influence of environment on the electronic structure of cob(III)alamins: Time-resolved absorption studies of the S<sub>1</sub> state spectrum and dynamics. *J. Am. Chem. Soc.* **2007**, *129*, 7578-7585.
- (63) Shiang, J. J.; Walker II, L. A.; Anderson, N. A.; Cole, A. G.; Sension, R. J. Time-resolved spectroscopic studies of B<sub>12</sub> coenzymes: The photolysis of methylcobalamin is wavelength dependent. *J. Phys. Chem. B* **1999**, *103*, 10532-10539.
- (64) Walker II, L. A.; Jarrett, J. T.; Anderson, N. A.; Pullen, S. H.; Matthews, R. G.; Sension, R. J. Time-resolved spectroscopic studies of B<sub>12</sub> coenzymes: The identification of a metastable cob(III)alamin photoproduct in the photolysis of methylcobalamin. *J. Am. Chem. Soc.* **1998**, *120*, 3597-3603.
- (65) Lodowski, P.; Jaworska, M.; Andruniow, T.; Kumar, M.; Kozlowski, P. M. Photodissociation of Co-C bond in methyl- and ethylcobalamin: An insight from TD-DFT calculations. *J. Phys. Chem. B* **2009**, *113*, 6898-6909.
- (66) Lodowski, P.; Jaworska, M.; Andruniow, T.; Garabato, B. D.; Kozlowski, P. M. Mechanism of Co–C bond photolysis in the base-on form of methylcobalamin. *J. Phys. Chem. A* **2014**, *118*, 11718-11734.
- (67) Karunakaran, V.; Benabbas, A.; Youn, H.; Champion, P. M. Vibrational coherence spectroscopy of the heme domain in the CO-sensing transcriptional activator CooA. *J. Am. Chem. Soc.* **2011**, *133*, 18816-18827.
- (68) Karunakaran, V.; Benabbas, A.; Sun, Y. H.; Zhang, Z. Y.; Singh, S.; Banerjee, R.; Champion, P. M. Investigations of low-frequency vibrational dynamics and ligand binding kinetics of cystathionine beta-synthase. *J. Phys. Chem. B* **2010**, *114*, 3294-3306.
- (69) Barabanschikov, A.; Demidov, A.; Kubo, M.; Champion, P. M.; Sage, J. T.; Zhao, J. Y.;

- Sturhahn, W.; Alp, E. E. Spectroscopic identification of reactive porphyrin motions. *J. Chem. Phys* **2011**, *135*, 015101.
- (70) Hoffman, D. P.; Mathies, R. A. Femtosecond stimulated raman exposes the role of vibrational coherence in condensed-phase photoreactivity. *Acc. Chem. Res.* **2016**, *49*, 616-625.
- (71) Milota, F.; Prokhorenko, V. I.; Mancal, T.; von Berlepsch, H.; Bixner, O.; Kauffmann, H. F.; Hauer, J. Vibronic and vibrational coherences in two-dimensional electronic spectra of supramolecular J-aggregates. *J. Phys. Chem. A* **2013**, *117*, 6007-6014.
- (72) Dean, J. C.; Scholes, G. D. Coherence spectroscopy in the condensed phase: Insights into molecular structure, environment, and interactions. *Acc. Chem. Res.* **2017**, *50*, 2746-2755.

For Table of Contents Only

